ELSEVIER

Materials Science and Engineering A 489 (2008) 337–350

MATERIALS SCIENCE & ENGINEERING A

www.elsevier.com/locate/msea

Microstructural development in porous β-Si_3N_4 ceramics prepared with low volume RE_2O_3–MgO–(CaO) additions (RE = La, Nd, Y, Yb)

Kevin P. Plucknett [a,*], Mervin Quinlan [a], Liliana Garrido [b], Luis Genova [c]

[a] *Materials Engineering Program, Department of Process Engineering and Applied Science, Dalhousie University, 1360 Barrington Street, Halifax, Nova Scotia, B3J 1Z1, Canada*

[b] *CONICET, Centro de Technologia de Recursos Minerales y Cerámica (CETMIC, CIC-CONICET-UNLP), Cam. Centenario y 506, C.C.49 (B 1897 ZCA) M.B. Gonnet. Pcia. De Buenos Aires, Argentina*

[c] *IPEN Instituto de Pesquisas Energéticas e Nucleares, CCTM Centro de Ciência e Technologia de Materiais, Cidade Universitária, Travessa R 400, 05508-900 São Paulo, Brazil*

Received 19 October 2007; received in revised form 14 December 2007; accepted 17 December 2007

Abstract

Porous β-Si_3N_4 ceramics have a wide range of potential applications, including filters for hot gases or molten metals, bioreactor supports and lightweight structural components. In the present study, a new approach is taken for the production of porous β-Si_3N_4 ceramics based on compositional design. A low volume fraction of *multiple* sintering aids is employed, where each additive is designed to play one or more specific roles in the sintering behavior and microstructural development of β-Si_3N_4 (e.g. densification, α- to β-Si_3N_4 transformation, anisotropic β-Si_3N_4 whisker growth, debonding aid). The primary aim of this work was to develop β-Si_3N_4 ceramics with a more porous microstructure than in prior work (ideally with 20–40 vol.% porosity), while developing high grain aspect ratios (i.e. >10:1) such that good mechanical performance can be expected. Compositions are based on various ratios of RE_2O_3:MgO, where RE = La, Nd, Y or Yb, with selected materials also prepared with small CaO additions. Sintering has been conducted in a nitrogen atmosphere (0.1 MPa), at temperatures between 1400 and 1700 °C. The influence of sintering aid composition and sintering temperature has been assessed. Particular attention was paid to microstructure development, including: densification behavior, retained pore size, the extent of α- to β-Si_3N_4 transformation, and the evolution of β-Si_3N_4 grain aspect ratios.

Keywords: Porous ceramics; Silicon nitride; Silicon oxynitride; Grain growth; Scanning electron microscopy

1. Introduction

There is growing international interest in the development of advanced porous ceramics for a wide range of applications, including use as filters, bio-prosthetic implants, bioreactor supports, and lightweight structural materials. Porous silicon nitride (Si_3N_4) ceramics possess a desirable combination of mechanical and thermal properties for such applications, particularly in the form of β-Si_3N_4, where highly anisotropic grain structures may be formed. A variety of approaches have been developed to prepare β-Si_3N_4 based ceramics with either nano-, micro- or macro-scale porosity [1–12]. Materials with nano-/micro-porosity, can be readily prepared by processing with a single sintering aid that promotes the α- to β-Si_3N_4 transformation, but has minimal beneficial effect on densification [1–6]. Suitable sintering aids for this approach include oxides of the lanthanide or Group III elements (e.g. La_2O_3, Lu_2O_3, Nd_2O_3, Sm_2O_3, Y_2O_3, Yb_2O_3, etc.); oxides of this type will be subsequently referred to by the generic term "rare earth oxides" (RE_2O_3). In this instance, a high viscosity Si–RE–O–N oxynitride glass phase is formed at the processing temperature, which retards densification but not the α- to β-Si_3N_4 transformation. Sintering in this instance is observed to be diffusion controlled [13]. This approach leads to materials with extremely fine scale porosity. The individual anisotropic β-Si_3N_4 grains form an interlocking network throughout the material, which provides good mechanical behavior. This general approach has been further refined, through the use of controlled seeding and texture development, including sinter-forging [11,12]. Strengths in excess of 1 GPa can be achieved for these materials, in combination with high toughness, although the retained porosity content is typically less than 15 vol.% [11].

* Corresponding author. Tel.: +1 902 494 3297; fax: +1 902 420 7639.
E-mail address: kevin.plucknett@dal.ca (K.P. Plucknett).

0921-5093/$ – see front matter © 2008 Elsevier B.V. All rights reserved.
doi:10.1016/j.msea.2007.12.023

Alternatively, macro-porosity can be controlled through the addition of fugitive pore formers, which can be either particulate (e.g. starch) or continuous in nature (e.g. open cell foams) [9,10]. Recently, processes based on suspension freezing have also been developed to form porous ceramics, where displacement of the ceramic powder occurs at the solidification front, resulting in interconnected porosity after sublimation of the suspension medium (e.g. water, camphene) [14]. This general approach has been utilized for Si_3N_4-based ceramics, primarily using aqueous based processing [15].

The present work reports upon a new approach to develop nano-/micro-porous β-Si_3N_4 ceramics. A low volume fraction of *multiple* sintering additives are used, where each additive component is selected to promote one or more of the following functions: (i) α- to β-Si_3N_4 phase transformation, (ii) anisotropic β-Si_3N_4 grain growth, or (iii) densification. The current approach is adapted from the prior work of Pyzik and colleagues, developing tough *in situ* reinforced β-Si_3N_4 ceramics [16,17]. If a specific role can be assigned to each individual additive when used in isolation during the sintering of β-Si_3N_4 ceramics, they can be plotted on a "functionality map", as shown in Fig. 1 (adapted from [16]). The location of each of the additives on the map is dictated by it role (or roles) during sintering, primarily when present as the *sole* sintering aid. As an example, an additive that contributes to each of functions (i)–(iii) will sit in the middle of the triangle, while one that only contributes to one role will sit in that respective corner. If a single RE_2O_3 addition contributes more to one function than another, its position in the centre is weighted to one or two corners. For the case of CaO, it is noted primarily on the functionality map that this additive contributes to anisotropic grain growth [16]. However, CaO additions are also observed to promote debonding of the β-Si_3N_4 grains in dense ceramics [17].

2. Experimental procedures

Ube SN E-10 α-Si_3N_4 powder was used for the preparation of all the samples in the current work. The oxide sintering additives used, including various RE_2O_3, together with their nominal purity as specified by the manufacturer, are summarized in Table 1. Table 2 outlines the Y_2O_3-containing compositions that where studied. For the case of the other RE_2O_3, they were supplemented for Y_2O_3 on a *molar equivalent* basis. Mixtures were prepared in 50 g batches of the appropriate compositions. The powders were first ball-milled for 24 h in isopropyl alcohol, using TZP media, after which they were dried and then crushed with a pestle and mortar. Powder mixtures were then uniaxially pressed (at ∼30 MPa) into 31.75 mm diameter × ∼4 mm thick discs, followed by vacuum bagging and cold-isostatic pressing at ∼175 MPa. Sintering of all the MgO containing samples was conducted within a protective powder bed, which was comprised of a mixture of 50 wt.% BN/49 wt.% Si_3N_4/1 wt.% MgO. All sintering was conducted within a high purity graphite crucible. In addition to the multi-additive samples, single rare earth oxide additive materials were also prepared (with a RE_2O_3 additive content of 3.2 mol.%). In this instance samples were sintered in a mixed 50 wt.% Si_3N_4/50 wt.% BN powder bed, again within a graphite crucible.

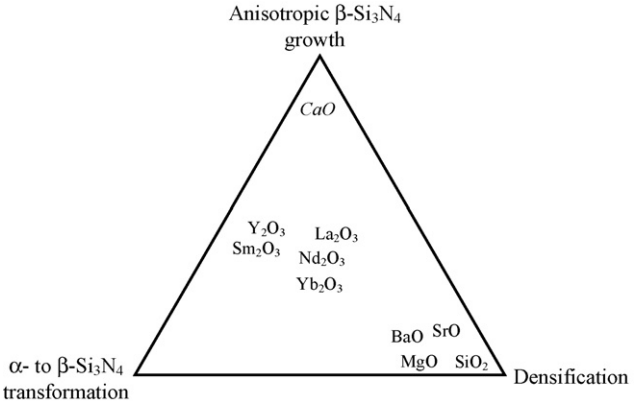

Fig. 1. Sintering aid functionality map (adapted from [16]), based on the use of each oxide as a single sintering additive for Si_3N_4 ceramics.

Table 1
Summary of the oxide sintering additives used, their purity and supplier

Sintering aid	Purity (at.%)	Supplier
La_2O_3	99.99	Metall Rare Earth Ltd., Shenzhen, China
Nd_2O_3	99.99	Treibacher Industries, Toronto, Canada
Y_2O_3	99.99	Metall Rare Earth Ltd., Shenzhen, China
Yb_2O_3	99.99	Treibacher Industries, Toronto, Canada
MgO	99.9	Inframat Advanced Materials, Farmington, CT
CaO	99.95	Alfa Aesar, Ward Hill, MA

After loading the crucible into the furnace, it was evacuated to ∼0.02 Torr, and then backfilled with nitrogen to ∼400 Torr, after which the chamber was again evacuated to ∼0.02 Torr. The sintering cycle involved heating the samples to 750 °C under dynamic vacuum (∼0.02 Torr), at a rate of 10 °C/min, and then holding at this temperature for 15 min. During this hold the furnace was back-filled with nitrogen to ∼750 Torr. A static nitrogen environment was maintained for the remainder of the sintering cycle, with the samples ramped to the final hold temperature at 10 °C/min. Sintering was performed at various temperatures between 1400 and 1750 °C for the multiple additive materials, and between 1500 and 1750 °C for the single additive compositions. In each case there was a hold period of 2 h at the final sintering temperature. During the hold the nitrogen

Table 2
Compositional designations for the porous Si_3N_4 samples prepared in the present work with Y_2O_3-based additions

Sample ID	Composition (wt.%)			
	Si_3N_4	Y_2O_3	MgO	CaO
5Y	95	5	–	–
YM	97	1.5	1.5	–
2YM	97	2	1	–
5YM	97	2.5	0.5	–
5YM01C	97	2.5	0.5	0.1
5YM05C	97	2.5	0.5	0.5

Note that samples with CaO additions are prepared with a baseline composition of 5YM. Alternate rare earth oxides, namely La_2O_3, Nd_2O_3 and Yb_2O_3, are substituted for Y_2O_3 on a direct molar equivalent basis.

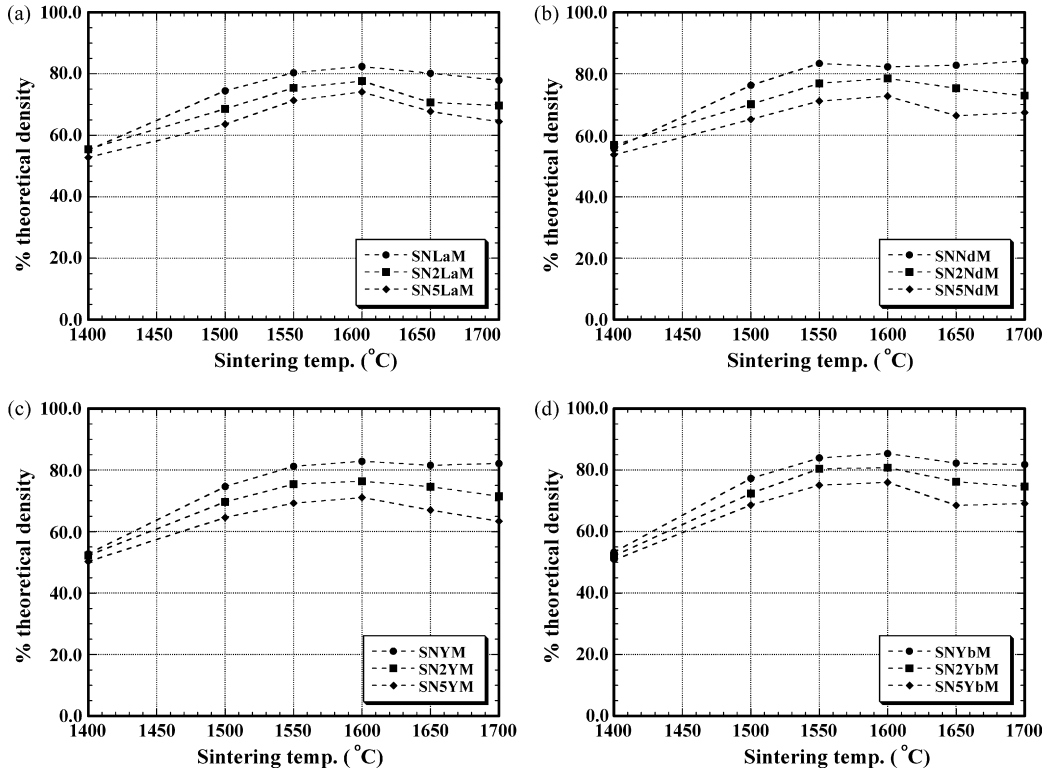

Fig. 2. Densification behavior for porous Si_3N_4 ceramics prepared with various mixed RE_2O_3–MgO sintering additives: (a) La_2O_3–MgO, (b) Nd_2O_3–MgO, (c) Y_2O_3–MgO, and (d) Yb_2O_3–MgO additions.

pressure increased to ~800 Torr, and it was subsequently maintained at this pressure through the use of a one-way pressure relief valve.

The sintered densities of samples were determined via immersion in mercury, due to the high retained porosity content. The pore size distribution of selected samples was determined using mercury intrusion porosimetry (Model Poremaster PM33-7, Quantachrome Instruments, Boynton Beach, Florida, USA). Post-sinter microstructural characterization was conducted on carbon-coated fracture surfaces using a field emission scanning electron microscope (FE-SEM; Model Hitachi S-4700, Hitachi High Technologies, Tokyo, Japan). Crystalline phase analysis was performed using X-ray diffraction (XRD; Model Bruker D-8 Advance, Buker Inc., Madison, WI). The fraction of β-Si_3N_4 formed, R_β, relative to residual α-Si_3N_4, was determined from XRD using the following relationship [18]:

$$R_\beta = \left[1.4434\left(\frac{I_\beta(1\,0\,1)}{I_\beta(1\,0\,1)+I_\alpha(2\,0\,1)}\right) - 0.4434\left(\frac{I_\beta(1\,0\,1)}{I_\beta(1\,0\,1)+I_\alpha(2\,0\,1)}\right)^2\right]$$

where an R_β value of 1.0 indicates full transformation to β-Si_3N_4, and an R_β value of 0.0 would indicate only α-Si_3N_4 was present; it should be noted that the Ube SN E-10 α-Si_3N_4 powder used in the present work typically contains 4–5 vol.% β-Si_3N_4.

After sintering, the β-Si_3N_4 grain aspect ratio was determined by partially dissolving small sections of material in a diluted HF solution (49% HF, diluted 5:1 with doubly distilled water), which primarily attacks the residual glass, followed by filtering of the resulting suspension. The particles were then ultrasonically dispersed in acetone, with the suspension subsequently dripped onto a polished and heated aluminum stub to rapidly evaporate the acetone. Finally, they were examined in the FE-SEM to determine the length and width of the individual grains, which were measured directly from digital micrographs.

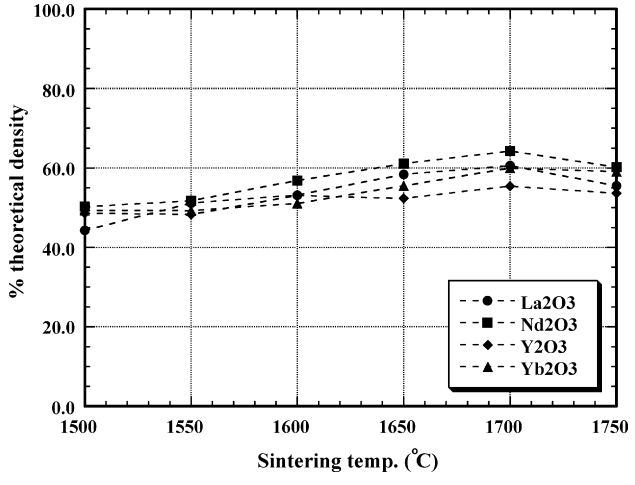

Fig. 3. Densification behavior for porous Si_3N_4 ceramics prepared with various single RE_2O_3 sintering additives (additive level 3.2 mol.%).

3. Results and discussion

3.1. Densification behavior

The influence of additive composition upon densification behavior is shown in Fig. 2a–d for samples prepared with varying RE_2O_3:MgO ratios. The effect of RE_2O_3-type on samples prepared with single additions (with 3.2 mol.% RE_2O_3) is shown in Fig. 3. It is readily apparent that single RE_2O_3 additions do not promote significant densification. This general behavior can be anticipated from prior studies [1–6,13], as a high viscosity Si–RE–O–N glass is formed at the sintering temperature, which does not allow significant particle rearrangement under the sintering conditions examined; typically, such compositions are densified by pressurized sintering methods such as hot-pressing, hot-isostatic pressing or gas-pressure sintering [19]. When examining the samples prepared with mixed RE_2O_3:MgO additions, it can be seen that increasing the MgO:RE_2O_3 ratio increases the level of densification in all cases; it should be noted that this compositional translation also results in a small increase in liquid volume, due to the lower density of MgO relative to the RE_2O_3 oxides, although this is anticipated to have minimal effect on densification. The residual porosity in these materials is invariably in the range of 20–40 vol.% (Fig. 2a–d). The additive levels for these samples are significantly lower than used for conventional pressureless-sintering of Si_3N_4-based ceramics to high density. In each of the examples shown in Fig. 2, there is a general decrease in sintered density above 1600 °C. Weight losses during sintering for all temperatures up to and including 1600 °C were less than 1 wt.%. It is notable that weight losses increased with sintering temperature above 1600 °C, such that at the highest sintering temperatures (i.e. 1650 and 1700 °C), weight losses ranged from 2 to 6 wt.% (Fig. 4a). It is likely that the small density reductions observed above 1600 °C are therefore a consequence of this volatilization. Slightly lower weight losses were observed for the single RE_2O_3 additions, even when sintering at 1750 °C for 2 h (Fig. 4b).

Previous studies of the physical properties of Si–Y–Mg–O–N glasses have demonstrated that increasing the Y_2O_3:MgO ratio results in an increase in both the glass transition temperature, T_g, and in the glass softening temperature [20]. This response is also expected to be demonstrated in the relative viscosity of such glasses, at any given temperature, with higher Y_2O_3:MgO ratios producing higher viscosity glasses. The effects of RE_2O_3:MgO ratio on glass properties have also

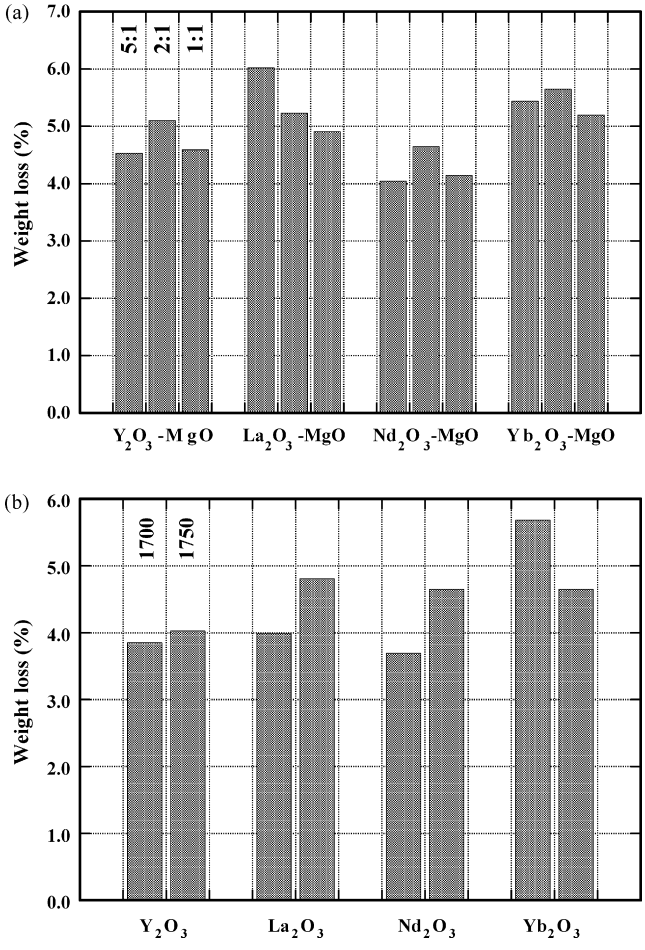

Fig. 4. (a) Weight loss of mixed RE_2O_3–MgO additive samples sintered at 1700 °C. (b) Weight loss of single RE_2O_3 additive samples sintered at 1700 and 1750 °C.

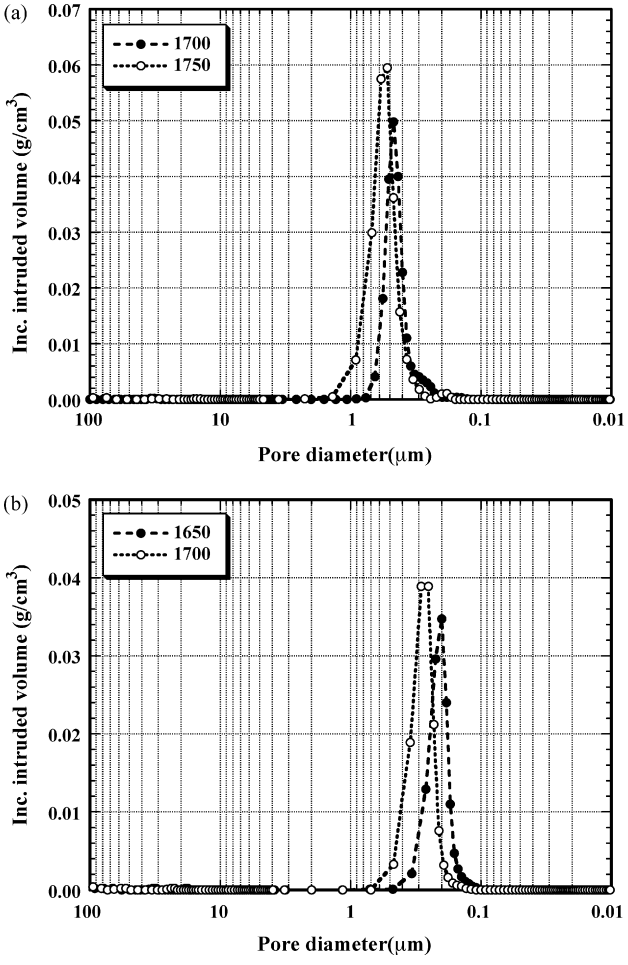

Fig. 5. Mercury intrusion pore size measurements for compositions prepared with (a) single Y_2O_3 additions (3.2 mol.%), sintered at 1700 and 1750 °C, and (b) a Y_2O_3:MgO ratio of 5:1, sintered at 1650 and 1700 °C.

been studied by Tredway and Loehman for Sc_2O_3-containing Mg–Si–O–N and Mg–Al–Si–O–N oxynitride glasses [21]. In that study it was demonstrated that increasing the Sc:Mg ratio increased the measured glass transition temperature, T_g. From these observations it can be inferred that the glass viscosity, at a constant temperature, will also be increased. A similar response in the present case would be seen as an increasing glass viscosity for the RE_2O_3:MgO additive samples in the ratio sequence 1:1 < 2:1 < 5:1, which correlates well with the decrease in sintered density with increasing RE_2O_3:MgO ratio shown in Fig. 2a–d.

In contrast, the data presented in Fig. 2a–d demonstrates that there is no clear trend in the effect of RE_2O_3-type upon the sintered densities, for mixed RE_2O_3–MgO additions. For example, increasing the ionic radius (and consequently decreasing the nominal cationic field strength (CFS), which is defined as the cation valence (Z) divided by the square of the cation radius (r_c), i.e. CFS $= Z/r_c^2$ [22]) does not have a clear influence on sintered density; Yb_2O_3–MgO gives marginally increased sintered densities relative to the other additives, while the response of the remaining three RE_2O_3–MgO systems is generally comparable. Similar observations can also be made for the single additive materials (Fig. 3), although in this instance slightly higher sintered densities are generally observed for the larger ionic radii systems (i.e. La_2O_3 and Nd_2O_3). It has previously been demonstrated for RE–Si–Al–O–N glasses, with a constant O:N ratio, that increased CFS results in an increased T_g and microhardness, and a reduced molar volume and thermal expansion coefficient [23]. The effects on glass viscosity were similar, in that increased CFS resulted in increased glass viscosity [23]. Essentially identical observations have also been made by Becher et al., when examining both RE–Si–Al–ON and RE–Si–Mg–O–N glasses [24,25]. It was shown in those studies that for nominally equivalent glasses, substituting La (r_c = 1.05 Å) for Lu (r_c = 0.85 Å) decreases the viscosity–temperature curves by approximately 30 °C [25]. From the perspective of densification behavior, it is apparent in the present work that the glass viscosity is influenced less by the RE_2O_3 chosen and more by the RE_2O_3:MgO ratio.

Typical examples of the retained pore size distribution for selected single and multi additive materials are shown in Fig. 5. It is apparent in each case that a nominally monomodal pore size distribution is present after sintering, with mean pore sizes in the range of 500–700 nm for single additive samples, prepared with 3.2 mol.% Y_2O_3, and 200–300 nm for the multiple additive samples, prepared with a Y_2O_3:MgO ratio of 5:1. In each of these cases, the data was obtained for materials that are fully transformed to β-Si_3N_4 (as noted in the following section). It is apparent that increased sintering temperature results in pore

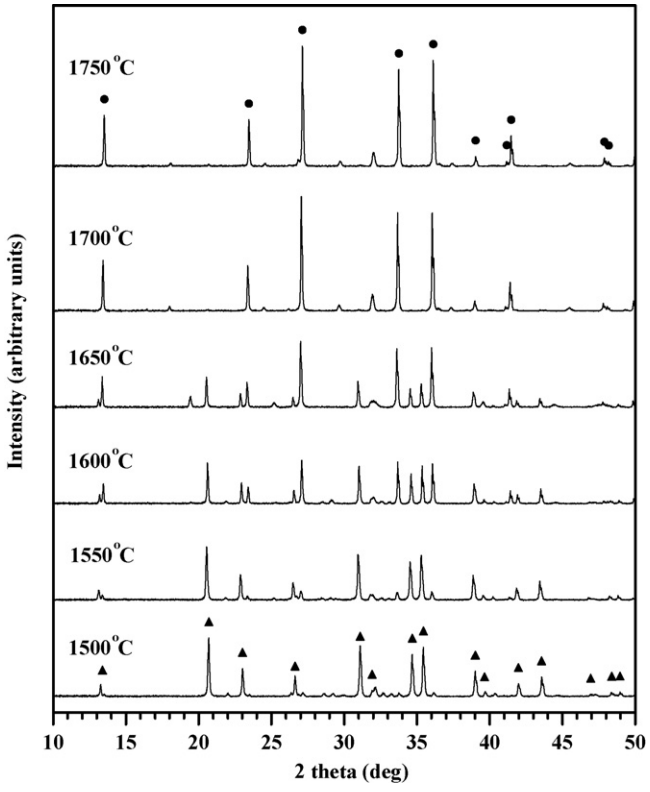

Fig. 6. Phase development as a function of sintering temperature for samples prepared with a single 3.2 mol.% Y_2O_3 addition (▲: α-Si_3N_4, ●: β-Si_3N_4).

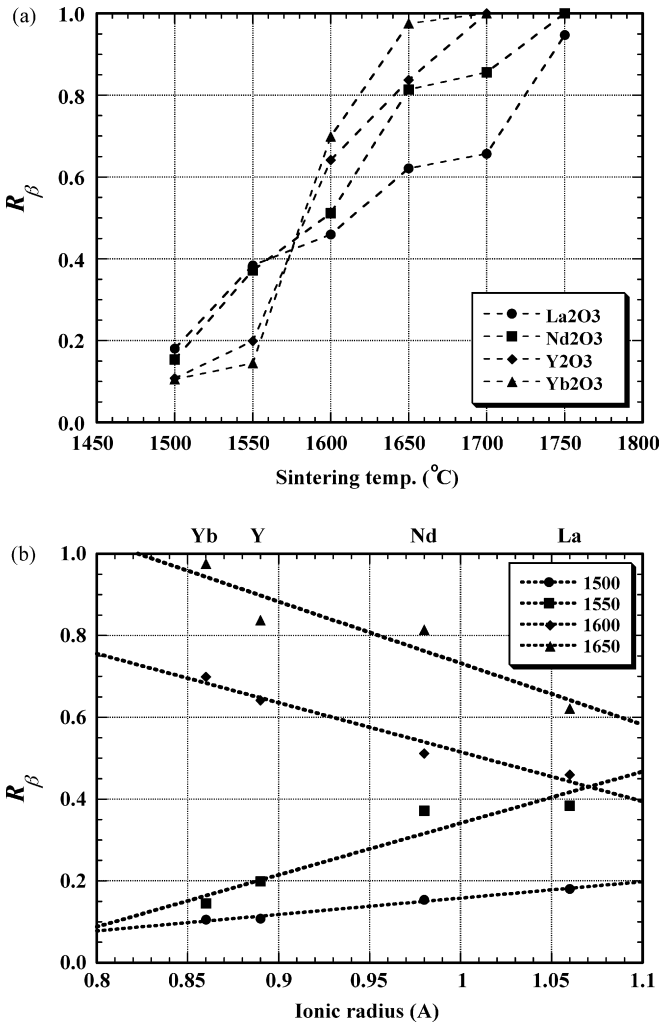

Fig. 7. (a) The fraction of α-Si_3N_4 transformed to β-Si_3N_4 (R_β) as a function of sintering temperature for porous Si_3N_4 prepared with single rare earth oxide additions. (b) The fraction of α-Si_3N_4 transformed to β-Si_3N_4 (R_β) as a function of rare earth ionic radius, for porous Si_3N_4 prepared with single rare earth oxide additions and sintered at temperatures between 1500 and 1650 °C.

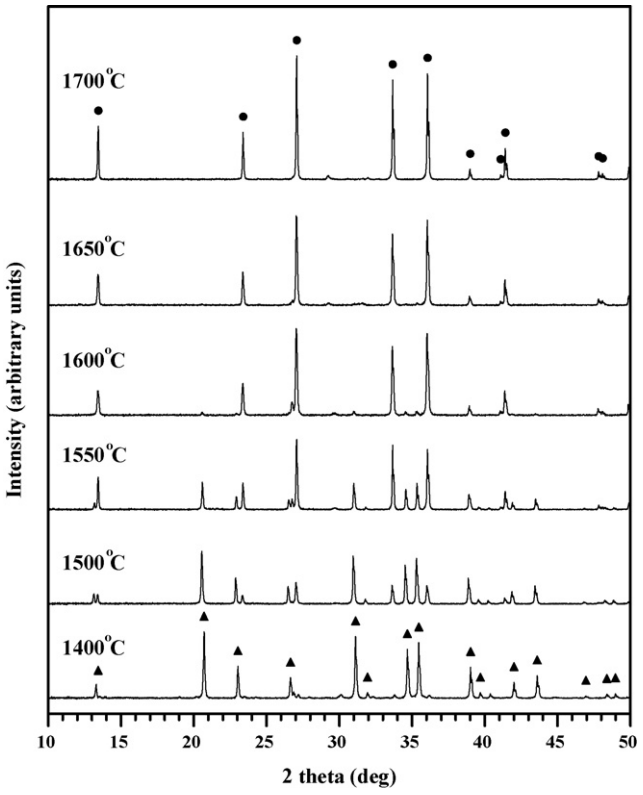

Fig. 8. Phase development as a function of sintering temperature for samples prepared with a $5Y_2O_3$:MgO ratio (▲: α-Si_3N_4, ●: β-Si_3N_4).

coarsening in both compositions, and therefore this allows a further means of tailoring the pore size distribution for fully transformed porous β-Si_3N_4 ceramics.

3.2. α- to β-Si_3N_4 transformation behavior

The effects of sintering temperature on the α- to β-Si_3N_4 transformation for the single additive material, prepared with 3.2 mol.% Y_2O_3, are presented in Fig. 6. It is apparent with this composition that essentially complete α- to β-Si_3N_4 transformation is achieved after sintering at 1700 °C for a period of 2 h. When using single additive RE_2O_3 sintering aids, the specific RE_2O_3 used has a significant effect on the degree of α- to β-Si_3N_4 transformation, as shown in Fig. 7a. It is notable for the case of Y_2O_3 and Yb_2O_3 that complete or near complete transformation is observed at 1700 °C, while for Nd_2O_3 and, in particular, La_2O_3 the α- to β-Si_3N_4 transformation is retarded significantly. Even after sintering at 1750 °C, residual α-Si_3N_4 is retained for samples prepared with 3.2 mol.% La_2O_3. Fig. 7b highlights the influence of the rare earth additive on the transformation behavior, showing the fraction of β-Si_3N_4 formed, R_β, as a function of the rare earth ionic radius, at various sintering temperatures between 1500 and 1650 °C. At the higher sintering temperatures (i.e. 1600 and 1650 °C), it can be seen that there is a strong correlation between the transformed fraction of the original α-Si_3N_4 and the ionic radius, with increasing ionic radius corresponding to a decreased transformed fraction. This behavior can, at least in part, be viewed in terms of the glass viscosity during sintering. While there are

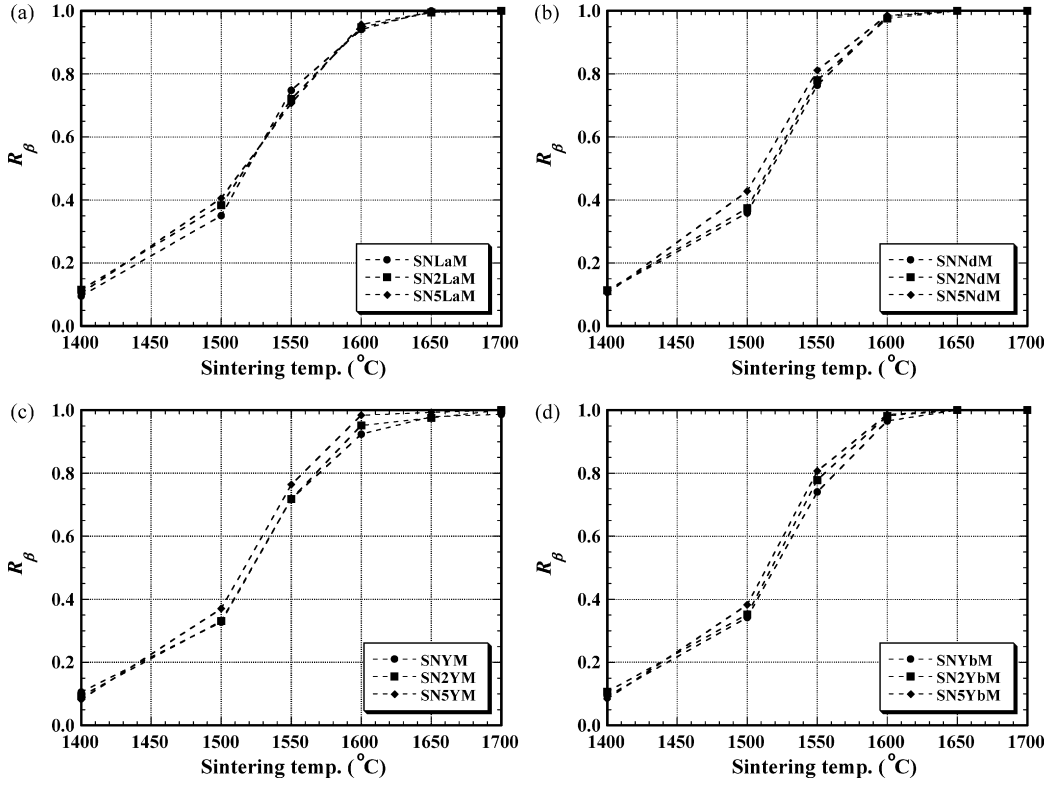

Fig. 9. The fraction of α-Si_3N_4 transformed to β-Si_3N_4 (R_β) as a function of sintering temperature for porous Si_3N_4 prepared with: (a) La_2O_3–MgO, (b) Nd_2O_3–MgO, (c) Y_2O_3–MgO, and (d) Yb_2O_3–MgO additions.

essentially no rheological studies on Si–RE–O–N glasses, there are several that address the high temperature rheology of both Si–RE–Al–O–N and Si–RE–Mg–O–N glasses [23–26]. In this prior work it is consistently noted that increasing ionic radius decreases glass viscosity, although by a relatively small amount. For the present case of Si–RE–O–N glasses, without MgO, this influence may be more pronounced. There is also a clear transition between the behavior at higher temperatures and that observed at 1550 °C (and to a lesser extent 1500 °C). Based on published phase equilibria, the binary eutectic temperatures for the RE_2O_3–SiO_2 systems being examined increase in the order [26–29]:

$$Nd_2O_3\text{–}SiO_2\,(1600\,^\circ C) < La_2O_3\text{–}SiO_2\,(1625\,^\circ C) < Yb_2O_3\text{–}SiO_2\,(1650\,^\circ C) < Y_2O_3\text{–}SiO_2\,(1660\,^\circ C)$$

Taking the Y_2O_3–SiO_2 binary system as an example, the addition of Si_3N_4 results in a lowering of the nominal eutectic temperature to ~1550 °C [30]. If similar reductions in eutectic temperature occur for the other RE_2O_3–SiO_2 systems, upon addition of Si_3N_4, it can be seen that for Nd_2O_3 and La_2O_3, Si–RE–O–N glass formation will occur near to 1500 °C, while for Yb_2O_3 and Y_2O_3 it will be closer to 1550 °C. This behavior correlates with the transition in behavior that is observed between 1550 and 1600 °C in Fig. 7b. At the lower temperatures, the transformation behavior is limited by the availability of a suitable Si–RE–O–N liquid phase, such that transformation is promoted with La_2O_3 or Nd_2O_3. However, at higher temperatures, liquid formation occurs in all four RE_2O_3 examples, and the α- to β-Si_3N_4 behavior is then dominated by the intrinsic rheological response of the liquid and, perhaps more importantly, the Si and N attachment kinetics. With this last point in mind, it has been demonstrated that the RE ion that is selected has a strong influence on the β-Si_3N_4 growth behavior [31–34]. For example, La_2O_3 promotes anisotropic growth, as Si and N attachment to the prism planes is reduced due to competition with the La for surface sites, while Yb_2O_3 tends to produce more equiaxial grains as Si and N attachment occurs more readily on the prism plane surfaces. Recent work by Becher et al. has demonstrated that this phenomenon tends to retard the α- to β-Si_3N_4 transformation when La_2O_3 is used as a sintering additive (in that instance in combination with MgO) [35], which is in good agreement with the results presented at the higher sintering temperatures in Fig. 7b.

The effects of MgO additions to Y_2O_3, on the α- to β-Si_3N_4 transformation behavior, are shown in Fig. 8. In comparison to the behavior with Y_2O_3 additions alone (Fig. 6), it is clear that MgO additions lower the α- to β-Si_3N_4 transformation temperature by approaching 100 °C. It is also readily apparent from Fig. 9a–d that the addition of MgO significantly lowers the transformation temperature in all the RE_2O_3–MgO materials, such that essentially complete α- to β-Si_3N_4 transformation is observed for the 5:1 ratio samples (SN5REM) when sintering at 1600 °C and above. In contrast to the case of single RE_2O_3 additions (Fig. 7a), for the multiple additive materials there is only minimal difference when comparing the different RE_2O_3–MgO systems. Similarly, increasing the relative content of MgO (i.e. decreasing the Y_2O_3:MgO ratio) results in only a slight reduction in the extent of α- to β-Si_3N_4 transformation for any given sintering temperature. Previous studies on Y–Si–Mg–O–N glasses have demonstrated that increasing the Y:Mg ratio results in an increase in both the glass transition and softening temperatures [20]. Similar observations to these have been made for the case of Sc–Si–Mg–(Al)–O–N glasses [21]. While direct viscosity data was not presented in either of these prior studies, it may be anticipated that the relative viscosity of such glasses will be affected in a similar manner at any given temperature. Increased viscosity may then be expected to decrease sintered density and increase the α- to β-Si_3N_4 transformation, following Hampshire and Jack [13]. However, it is clear that in the present case that this effect is subtle, as there is only minimal reduction in transformation rate with decreasing RE_2O_3:MgO ratio. The general conclusion must therefore be that the viscosity differences for RE–Si–Mg–O–N glasses must be small at typical sintering temperatures, such that transformation behavior is largely independent of RE_2O_3-type or

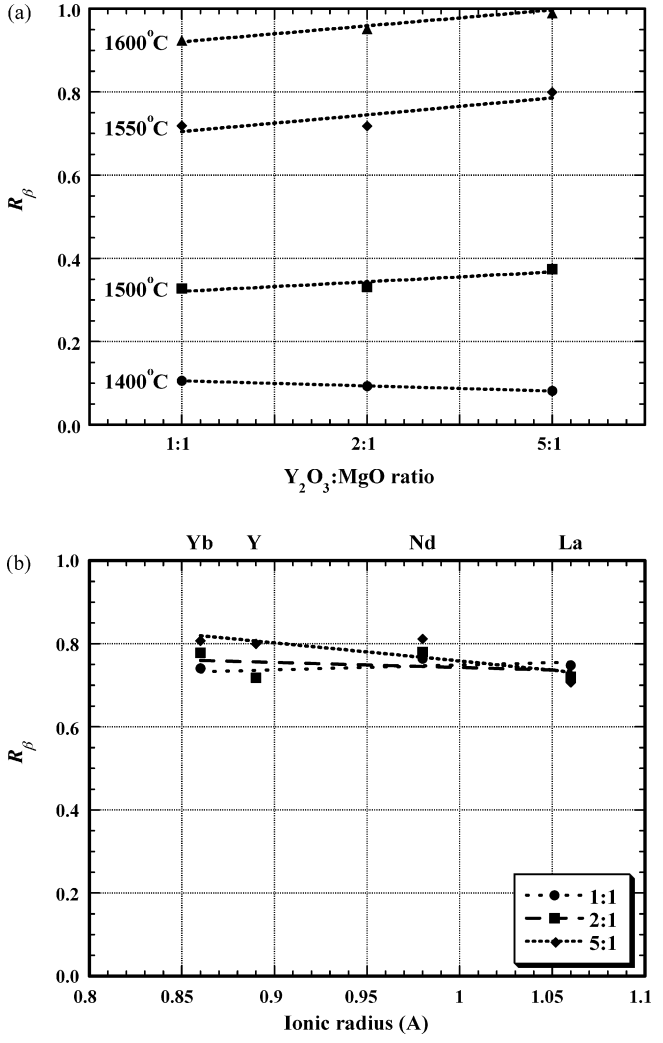

Fig. 10. (a) The fraction of β-Si_3N_4 formed as a function of sintering temperature for the three Y_2O_3:MgO ratios examined. (b) The fraction of β-Si_3N_4 formed after sintering at 1550 °C, as a function of RE ionic radius for the three RE_2O_3:MgO ratios examined.

the RE_2O_3:MgO ratio. This is highlighted in Fig. 10a, where the effects of Y_2O_3:MgO ratio are compared, after sintering at various temperatures between 1400 and 1600 °C. It can be seen that there is only minor difference in behavior, especially with a typical measuring error that can be associated with XRD (i.e. ±2 vol.%). If there is a slight trend in this data, it is that it shows similarities in nature to Fig. 7b, in that the highest Y_2O_3:MgO ratio (5:1) exhibits the lowest amount of transformation at 1400 °C, but the highest at 1600 °C. A similar liquid eutectic temperature/viscosity argument is likely to hold in this instance, as well as for the single additive materials, however, the effect is subtle at most. When examining the behavior of the different RE_2O_3 used, a similar lack of dependency is apparent (Fig. 10b); samples in this instance are all sintered at 1550 °C for 2 h.

In a recent study aimed at development of high toughness β-Si_3N_4 ceramics, it was shown that increasing RE ionic radius decreases the rate of α- to β-Si_3N_4 transformation, when examining materials prepared by hot-pressing with 8 wt.% RE_2O_3 and 2 wt.% MgO, where RE = Lu, Gd and La [35]. The indication from that work is that for La the prism plane attachment of Si and N to β-Si_3N_4 grains is retarded in comparison to Gd and Lu, in particular. Consequently, α- to β-Si_3N_4 transformation occurs primarily through Si and N attachment to the basal plane with La, and to both the prism planes and the basal plane with Gd and, especially, Lu. The α- to β-Si_3N_4 transformation is therefore slowed with the larger ionic radius La additions. In the present case this behavior is not apparent, as all RE_2O_3–MgO combinations behave in a similar manner (Fig. 9a–d). However, it must be remembered that the La additive concentration is approximately three to six times lower in the present work (depending on RE_2O_3:MgO ratio), such that the La effect may be largely suppressed, as there is only a limited concentration of La available for prism plane site attachment.

3.3. Microstructural development

The microstructural development of single additive materials prepared with various additive concentrations have been discussed in detail in a previous publication [36] and, as a consequence, will only be briefly discussed here. Fig. 11 demonstrates the typical microstructures obtained for the four RE_2O_3 single additive systems (3.2 mol.% additions) after sintering at 1750 °C for 2 h. It is apparent that a general microstructural coarsening occurs for the Yb_2O_3 additions in particular, and that the Nd_2O_3 and La_2O_3 additive materials exhibit qualitatively higher β-Si_3N_4 aspect ratios. It is important to remember in this instance that the La_2O_3 additive samples still contain a small portion of α-Si_3N_4, even after sintering at 1750 °C (Fig. 7a).

The influence of sintering temperature on microstructural development, for a Y_2O_3:MgO ratio of 5:1, is demonstrated in Fig. 12a–e. A transition from the fine, equiaxed α-Si_3N_4 morphology to the elongated β-Si_3N_4 structure is clearly apparent above 1600 °C. As noted earlier, these compositions are essentially fully transformed to β-Si_3N_4 at this temperature. Coarsening of this composition is also apparent with increasing sintering temperature above 1600 °C (e.g. Fig. 12c–e). When

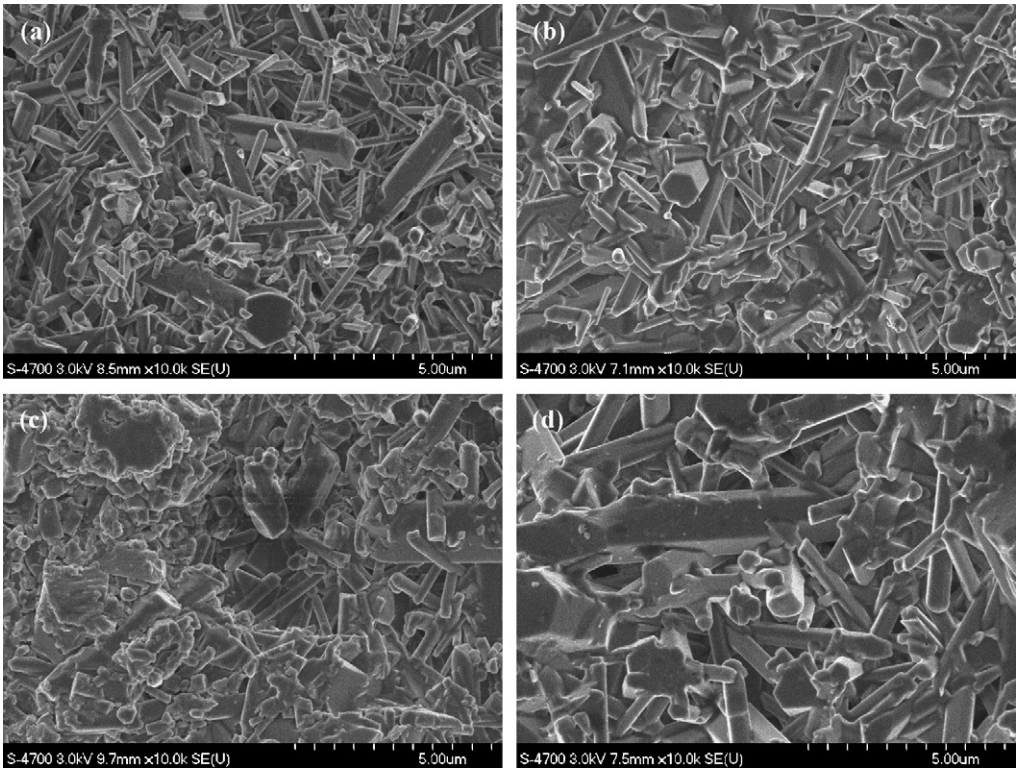

Fig. 11. FE-SEM images of β-Si_3N_4 ceramics sintered at 1750 °C for 2 h and prepared with single RE_2O_3 additions (3.2 mol.%): (a) La_2O_3, (b) Nd_2O_3, (c) Y_2O_3 and (d) Yb_2O_3.

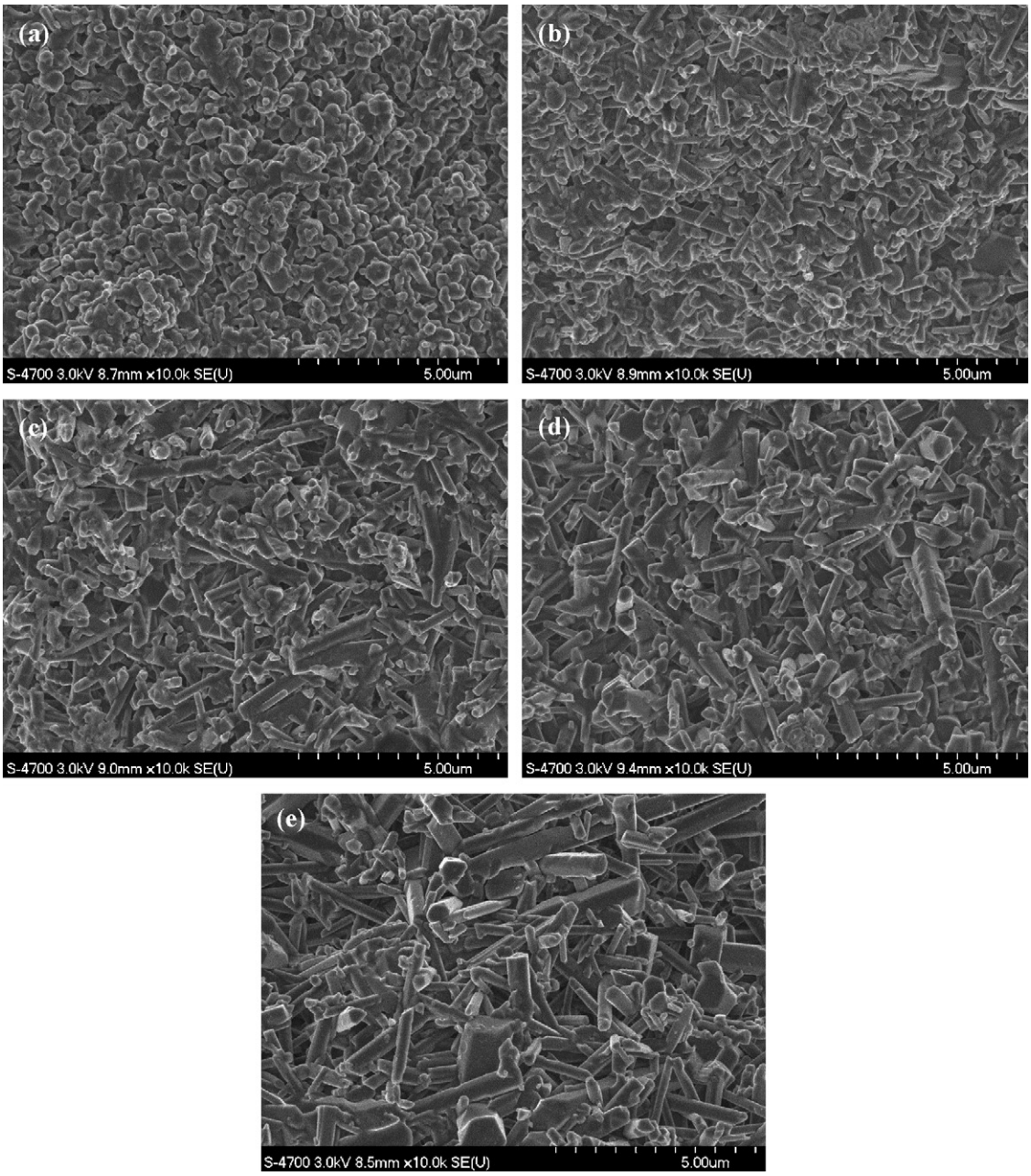

Fig. 12. SEM images of microstructural evolution for the composition SN5YM (i.e. Y_2O_3:MgO ratio of 5:1) sintered at (a) 1500 °C, (b) 1550 °C, (c) 1600 °C, (d) 1650 and 1700 °C. The change from equiaxial α-Si_3N_4 to elongated β-Si_3N_4, with increasing temperature, is readily apparent.

examining the effects of Y_2O_3:MgO ratio upon the sintered microstructure, it is again qualitatively apparent that decreasing the RE_2O_3:MgO ratio results in coarsening of the β-Si_3N_4 grains (Fig. 13; cf. Fig. 12e); samples in this instance were processed at 1700 °C for 2 h. As a consequence of this general observation, in combination with the increased sintered densities observed with the higher MgO containing samples, the 5:1 RE_2O_3:MgO ratio compositions were selected for further study of grain growth behavior, specifically aspect ratio development. This included the addition of small amounts of CaO which may potentially increase additional anisotropic β-Si_3N_4 grain growth, as outlined in Fig. 1, as well as promoting debonding of the β-Si_3N_4 grains [16,17].

Qualitatively, it was apparent that grain dimensions are quite different when comparing the various RE_2O_3:MgO examples, prepared with a 5:1 ratio, with narrower β-Si_3N_4 grains occurring when using La_2O_3 (Fig. 14). When comparing these observations with Yb_2O_3 and Nd_2O_3, it was noted that they behaved similarly to Y_2O_3 and La_2O_3, respectively. In accordance with the qualitative observations noted in Figs. 12 and 14, direct measurement of the grain dimensions for the samples prepared with a 5:1 ratio of RE_2O_3:MgO, sintered at 1700 °C, exhibited a clear increase in aspect ratio with increasing rare earth ionic radius (Figs. 15 and 16). The grain size distributions for the La_2O_3:MgO and Yb_2O_3:MgO highlight a transition from smaller, higher aspect ratio β-Si_3N_4 grains to ones that are larger

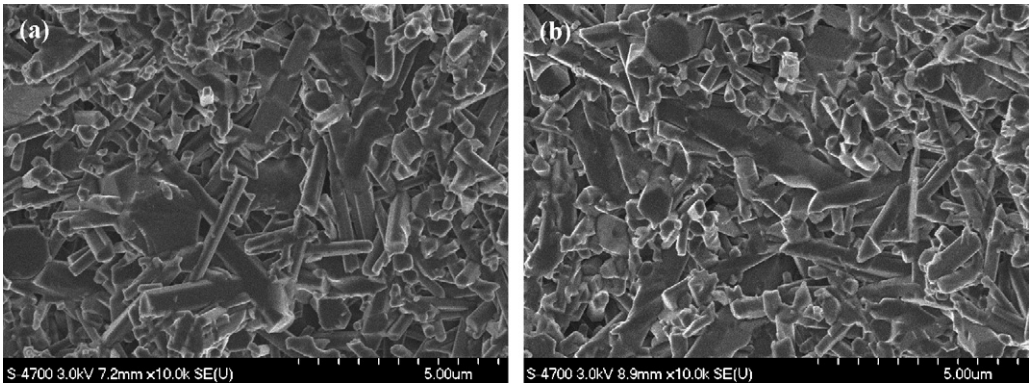

Fig. 13. SEM micrographs of the structure of (a) composition SN2YM (i.e. Y_2O_3:MgO ratio of 2:1) and (b) composition SNYM (i.e. Y_2O_3:MgO ratio of 1:1); both examples were sintered at 1700 °C for 2 h.

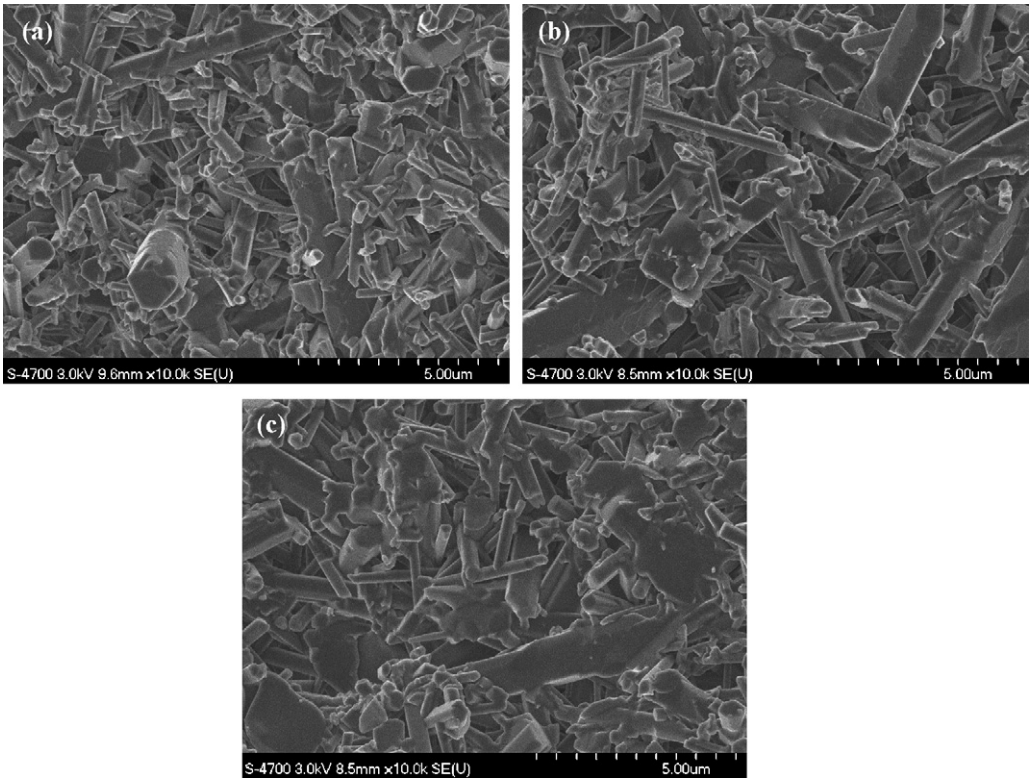

Fig. 14. FE-SEM images of β-Si_3N_4 ceramics sintered at 1700 °C for 2 h and prepared with (a) La_2O_3–MgO, (b) Nd_2O_3–MgO and (c) Yb_2O_3–MgO additions. In each example, an RE_2O_3:MgO ratio of 5:1 was used (c.f. SN5YM sintered at 1700 °C, shown in Fig. 11e).

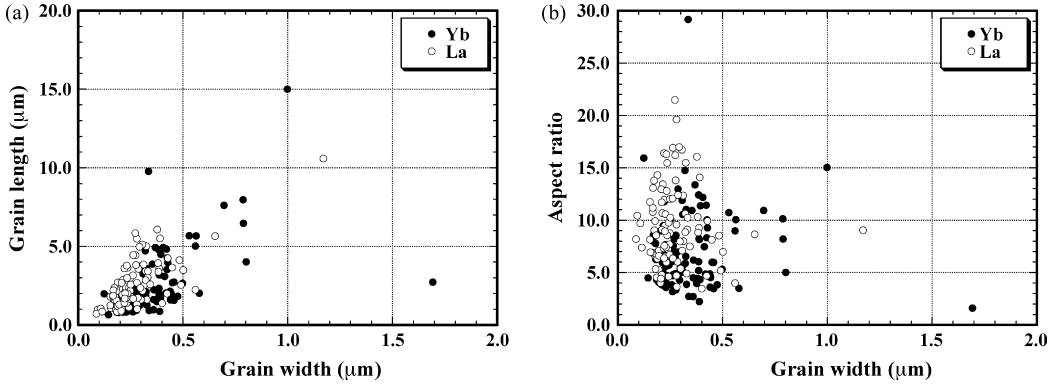

Fig. 15. (a) The measured length–width distributions for β-Si_3N_4 grains in compositions SN5YbM and SN5LaM sintered at 1700 °C. (b) The measured aspect ratio–width distributions for β-Si_3N_4 grains in compositions SN5YbM and SN5LaM sintered at 1700 °C.

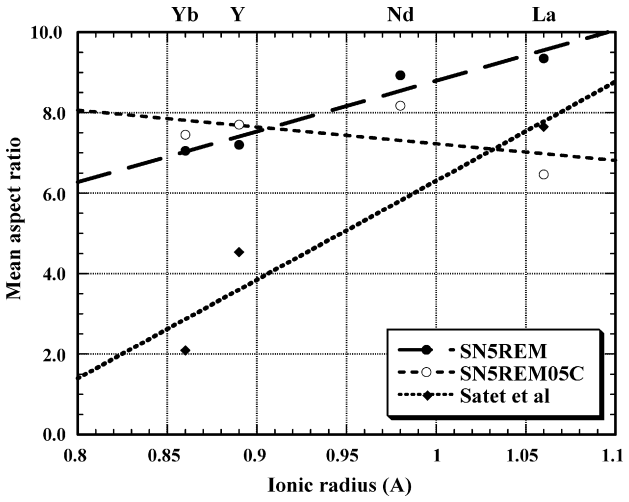

Fig. 16. The mean aspect ratio of β-Si_3N_4 grains as a function of RE_2O_3 cation radius. Samples were prepared at 1700 °C for 2 h, with a RE_2O_3:MgO ratio of 5:1, both without and with 0.5 wt.% CaO addition. Data from Satet et al. is shown for comparison [39,40].

and of lower aspect ratio, when Yb_2O_3 is substituted for La_2O_3 (Fig. 15). This transition is particularly clear when examining the mean aspect ratio as a function of RE ionic radius, with an increase in mean aspect ratio from ∼7:1 for Yb_2O_3:MgO to 9:1 for La_2O_3:MgO (Fig. 16); it should be noted that the aspect ratio values for Y_2O_3:MgO are lower than previously reported for these compositions [37], as it has been subsequently determined that the β-Si_3N_4 grains in that previous work were over-etched due to the use of concentrated HF solution for glass dissolution.

Several authors have assessed the grain growth kinetics of β-Si_3N_4 grains within RE–Si–Mg–O–N oxynitride glasses [38–41]. Saito et al. measured typical mean grain aspect ratios of ∼3:1 to 4:1 for dilute β-Si_3N_4 grains growing within Si–RE–Mg–O–N glasses, where RE = Gd, Nd and Y, and between 8:1 and 13:1 for RE = La, for samples prepared at 1500 °C [38]. The reasons for this behavior are unclear, although it should be noted that the processing temperature that was applied was relatively low (1500 °C) and that residual α-Si_3N_4 was invariably apparent, even after more than 500 min of heat-treatment. The α- to β-Si_3N_4 transformation behavior was reported for the Si–Y–Mg–O–N only in that work, so the extent of transformation for the remaining RE_2O_3 additions is unclear. Satet and Hoffman reported aspect ratios of ∼2:1 for a Yb–Si–Mg–O–N glass, rising to ∼7.5:1 for a comparable glass composition with La replacing Yb [39,40]. Their work highlighted a correlation of grain aspect ratio with ionic radius, although differing dependencies were observed for lanthanide (Lu, Yb, Sm, (La)) and Group III elements (Sc, Y, (La)). In the present case the grain aspect ratios are generally higher, especially for the case of the smaller ionic ratio compositions, and there is a lowered dependence on ionic radius, although it is still clearly present.

There are three potential reasons for the higher aspect ratios in the present instance, two of which relate to the relative β-Si_3N_4:glass volume ratio. Firstly, in the present examples the glass volume fraction is much less than the β-Si_3N_4 fraction, while in the prior studies the opposite is true. As a consequence, the "sink" of glass forming cationic material is much smaller. Examination of the microstructure of these materials at moderately high magnifications indicates that the residual glass may be primarily located at β-Si_3N_4 grain–grain contact points (Fig. 17). By the very nature of the growth, these regions are more predominantly the ends of the grains (i.e. the basal plane). Clearly, even if a residual glass component is present on the prism surfaces of the β-Si_3N_4 crystals, there is still a considerable diffusion distance (on an atomic scale) to replenish Si and N incorporated at the growth front. Secondly, it is important to remember that these materials are porous, and that the porosity is largely interconnected. As a consequence, vapor phase transport cannot be discounted as contributing to anisotropic β-Si_3N_4 growth. It has been recently noted that decreasing the green density in materials sintered with combined Y_2O_3, MgO and CaO additions results in higher β-Si_3N_4 aspect ratios at a constant sintering temperature [42]. However, it is important to note that this observation may be indicative of either vapor-phase transport or a reduction in the hindrance of β-Si_3N_4 growth. Evidence for growth hindrance, even in the present relatively porous materials, is readily apparent in Fig. 17. Similarly, in the preparation of dense β-Si_3N_4, isolated pores are often retained that contain large grains on their internal surfaces that have grown through vapor phase transport; in this instance the system can

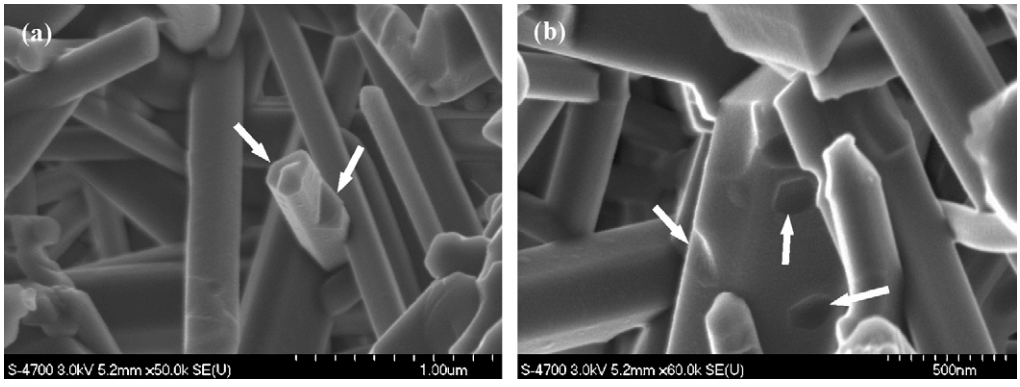

Fig. 17. High magnification FE-SEM images of the microstructure of composition SN5YM, demonstrating (a) hindrance of β-Si_3N_4 grain growth (arrowed), and (b) "failed" β-Si_3N_4 grain–grain contact points (arrowed).

Table 3
The effects of CaO additions upon the sintering behavior of the baseline composition 5YM at 1650 °C

Composition	Weight loss (%)	Sintered density (g cm^{-3})	Nominal retained porosity (vol.%)
5YM	2.52	2.15	33.2
5YM01C	1.33	2.28	28.9
5YM05C	1.37	2.29	28.8

be considered sealed when the surrounding matrix is fully densified. Further work is required to determine the mechanism responsible for higher aspect ratios in an unambiguous manner.

The mechanism of anisotropic β-Si_3N_4 grain growth has been the focus of significant recent attention, from both an experimental and theoretical perspective [31–35]. It has been postulated that, based upon calculation of the differential binding energy, there is increasing tendency for the adsorption of RE to the prism planes of β-Si_3N_4 with increasing ionic radius, which reduces the probability of Si and N attachment [31–35]. In accordance with these calculations, high-resolution transmission electron microscopy studies have demonstrated that cation attachment to the prism planes does occur [33,34]. As a consequence, there is a lowered tendency for β-Si_3N_4 grains to growth in directions perpendicular to the *c*-axis. Conversely, growth in the *c*-direction is unhindered, and therefore anisotropic growth is favored. This general trend is apparent in the present work, although the difference in measured aspect ratio, as a function of RE_2O_3 cation radius, is significantly less than noted for the case of more dilute β-Si_3N_4 systems [39–41]. This may simply be a result of growth hindrance phenomena, such that for the present materials the growth of higher β-Si_3N_4 aspect ratio grains in the La_2O_3:MgO materials is restricted by the surrounding grains. It is notable from a separate study of the composition SN5YM05C, milled for varying amounts of time, that measured aspect ratios are increased when samples are only uniaxially pressed at ~30 MPa, rather than subsequently cold-isostatically pressed at 175 MPa [42]. However, it is also possible that the effective additive cation dilution in the present system (discussed in the previous section), relative to prior studies of dense β-Si_3N_4 ceramics and oxynitride glasses containing low volume fractions of β-Si_3N_4, means that growth restrictions perpendicular to the *c*-axis are largely removed as there are simply insufficient RE species to inhibit Si and N attachment.

3.4. Effects of CaO additions

The effects of small CaO additions on the densification behavior of the Y_2O_3:MgO (5:1 ratio) composition, when sintering at 1650 °C for 2 h, are shown in Table 3. It is apparent that incorporation of even low CaO additions produce a significant increase in densification, although the porosity content after sintering at this temperature still exceeds 20 vol.%. Such behavior can be expected, since CaO additions will further lower the glass viscosity at typical sintering temperatures, resulting in increased densification. In conjunction with this behavior, the addition of CaO was also observed to reduce sintering weight losses, due to the formation of a lower porosity structure (Table 3).

As noted in the previous section, the initial aim of adding CaO to the 5:1 ratio RE_2O_3:MgO compositions was to promote anisotropic β-Si_3N_4 grain growth during sintering. Measurement of the grain dimensions after sintering both the Y_2O_3:MgO and Yb_2O_3:MgO compositions at 1700 °C demonstrates that CaO incorporation does increase the grain aspect ratio (Fig. 16), although the effect is relatively small. Conversely, there is actually a decrease in the aspect ratios measured for both the Nd_2O_3:MgO and, in particular, the La_2O_3:MgO systems. This may be attributed to grain coarsening when CaO is added lowering the eutectic temperature, although it is presently unclear why the effects are more significant for the La-based composition. Direct comparison of the effects of sintering temperature were made for the 5:1 ratio Y_2O_3:MgO additive, prepared with 0.5 wt.% CaO, and sintered at 1650 and 1700 °C (Fig. 18). In this instance there is a clear coarsening of the β-Si_3N_4 grains when sintering at the higher temperature, and a lower aspect ratio arises; the mean aspect ratios were 8.3 and 7.7, for the samples prepared at 1650 and 1700 °C, respectively. In general it appears that CaO does not result in significant increases in the

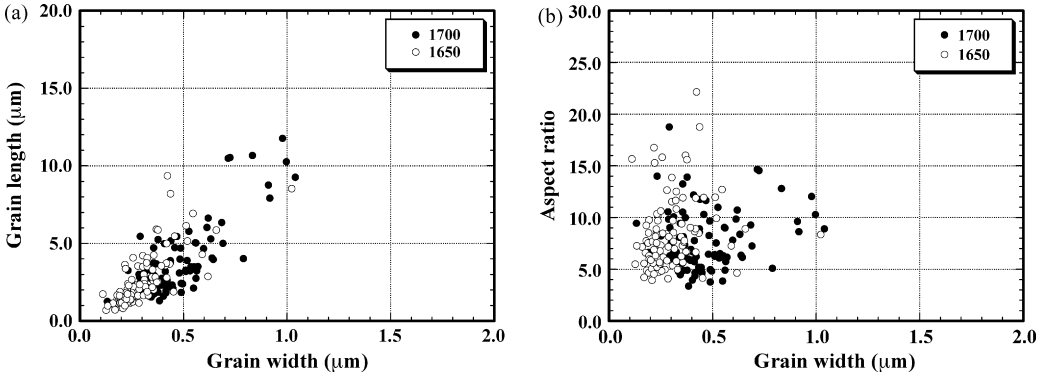

Fig. 18. (a) The measured length–width distributions for β-Si_3N_4 grains in composition SN5YM05C, sintered at 1650 or 1700 °C for a period of 2 h. (b) The measured aspect ratio–width distributions for β-Si_3N_4 grains in composition SN5YM05C, sintered at 1650 or 1700 °C for a period of 2 h.

β-Si_3N_4 grain aspect ratio, and that it is not an especially effective whisker growth agent in the present environment. Further study is needed to assess the behavior at lower sintering temperatures (i.e. 1600 °C), where full α- to β-Si_3N_4 transformation is still achieved with CaO additions. In this instance coarsening is likely to be suppressed, and higher grain aspect ratios should be achieved.

4. Conclusions

The current study has demonstrated that porous β-Si_3N_4 based ceramics can be prepared using a low volume fraction of multiple sintering additives (i.e. RE_2O_3 and MgO, where RE = La, Nd, Y or Yb). Potentially, this methodology has benefits over prior methods to prepare porous Si_3N_4 ceramics, in that the additives could be selected based on their specific "functionality" during sintering (e.g. densification aid, transformation aid, whisker growth agent, etc.). It has been shown that through this approach, the density (porosity) can be tailored, and that moderately high aspect ratios can be achieved through the addition of oxides known to promote β-Si_3N_4 whisker growth. However, it is also apparent that when used in combination with MgO, the relative variation in functionality of the different RE_2O_3 additions is minimized. For example, when used alone the extent of α- to β-Si_3N_4 phase transformation is highly dependent upon the RE_2O_3 selected, while the addition of MgO largely eliminates this RE_2O_3 dependency. It was also apparent that the α- to β-Si_3N_4 phase transformation was achieved at lower temperatures for multi-component systems, relative to single additive materials. Higher β-Si_3N_4 aspect ratios are achieved with higher ionic radii cations, such as La, in accordance with previous studies of dilute β-Si_3N_4 grains growing in a high volume RE–Si–Mg–O–N glass. However, the addition of CaO does not result in significantly increased β-Si_3N_4 whisker growth, and in some cases actually reduces the extent of anisotropic growth, contrary to initial expectations. Based on the presented work, *combined* compositional and microstructural design approaches are currently being evaluated, in order to promote high aspect ratio β-Si_3N_4 whisker growth; this work, together with an associated property evaluation, will be reported in a future publication.

Acknowledgements

The authors would like to acknowledge NSERC (Canada), CONICET (Argentina) and CNPq (Brazil) for provision of research funding through the Inter-American Research in Materials (CIAM) program. We also acknowledge the support of the Canada Foundation for Innovation, the Atlantic Innovation Fund, and other partners who helped fund the Facilities for Materials Characterisation, managed by the Dalhousie University Institute for Materials Research, who provided access to the FE-SEM. Mr. Brian Liekens (Department of Civil and Resource Engineering, Dalhousie University) is also gratefully thanked for performing the mercury porosimetry measurements.

References

[1] K.P. Plucknett, M.H. Lewis, J. Mater. Sci. Lett. 17 (1998) 1987–1990.
[2] N. Kondo, Y. Inagaki, Y. Suzuki, T. Ohji, Mater. Sci. Eng. A335 (2002) 26–31.
[3] J.-F. Yang, Z.-Y. Deng, T. Ohji, J. Eur. Ceram. Soc. 23 (2003) 371–378.
[4] N. Kondo, Y. Inagaki, Y. Suzuki, T. Ohji, J. Ceram. Soc. Jpn. 112 (2004) 316–320.
[5] J. Yang, J.-F. Yang, S.-Y. Shan, J.-Q. Gao, T. Ohji, J. Am. Ceram. Soc. 89 (2006) 3843–3845.
[6] Y. Inagaki, Y. Shigegaki, M. Ando, T. Ohji, J. Eur. Ceram. Soc. 24 (2004) 197–200.
[7] Z.-Y. Deng, Y. Inagaki, J. She, Y. Tanaka, Y.-F. Liu, M. Sakamoto, T. Ohji, J. Am. Ceram. Soc. 88 (2005) 462–465.
[8] Y. Inagaki, N. Kondo, T. Ohji, J. Eur. Ceram. Soc. 22 (2002) 2489–2494.
[9] A. Diaz, S. Hampshire, J. Eur. Ceram. Soc. 24 (2004) 413–419.
[10] A. Diaz, S. Hampshire, J.-F. Yang, T. Ohji, S. Kanzaki, J. Am. Ceram. Soc. 88 (2005) 698–706.
[11] N. Kondo, Y. Suzuki, T. Ohji, J. Mater. Res. 16 (2001) 32–34.
[12] Y. Inagaki, T. Ohji, S. Kanzaki, Y. Shigegaki, J. Am. Ceram. Soc. 83 (2000) 1807–1809.
[13] S. Hampshire, K.H. Jack, in: F.L. Riley (Ed.), Progress in Nitrogen Ceramics, Martinus Nijhoff Publishers, The Hague, 1983, pp. 225–230.
[14] K. Araki, J.W. Halloran, J. Am. Ceram. Soc. 87 (2004) 1859–1863.
[15] T. Fukasawa, Z.Y. Deng, M. Ando, T. Ohji, S. Kanzaki, J. Am. Ceram. Soc. 85 (2002) 2151–2155.
[16] A.J. Pyzik, D.F. Carroll, C.J. Hwang, in: I.-W. Chen, P.F. Becher, M. Mitomo, G. Petzow, T.-S. Yen (Eds.), Silicon Nitride Ceramics: Scientific and Technological Issues, Materials Research Society Symposium Proceedings, vol. 287, Materials Research Society, Boston, 1993, pp. 411–416.
[17] A.J. Pyzik, D.R. Beaman, J. Am. Ceram. Soc. 76 (1993) 2737–2744.
[18] T. Hirata, K. Akiyama, T. Morimoto, J. Eur. Ceram. Soc. 20 (2000) 1191–1195.
[19] O. Yeheskel, Y. Geffen, M. Talianker, J. Mater. Sci. 19 (1984) 745–752.
[20] M.J. Pomeroy, C. Mulcahy, S. Hampshire, J. Am. Ceram. Soc. 86 (2003) 458–464.
[21] W.K. Tredway, R.E. Loehman, J. Am. Ceram. Soc. 68 (1985) C-131–C-133.
[22] W. Vogel, in: N. Kreidl (Ed.), Chemistry of Glass, The American Ceramic Society, Westerville, OH, 1985.
[23] R. Ramesh, E. Nestor, M.J. Pomeroy, S. Hampshire, J. Eur. Ceram. Soc. 17 (1997) 1933–1939.
[24] P.F. Becher, S.B. Waters, C.G. Westmoreland, L. Riester, J. Am. Ceram. Soc. 85 (2002) 897–902.
[25] P.F. Becher, M.J. Lance, M.K. Ferber, M.J. Hoffmann, R.L. Satet, J. Non-Cryst. Solids 333 (2004) 124–128.
[26] N.A. Toropov, I.A. Bondar, Izv. Akad. Nauk SSSR, Otd. Khim. Nauk 5 (1961) 740.
[27] N.A. Toropov, Trans. 7th Int. Ceram. Congr., London, 1960, p. 440.
[28] N.A. Toropov, I.A. Bondar, Izv. Akad. Nauk SSSR, Otd. Khim. Nauk 4 (1961) 547.
[29] N.A. Toropov, I.A. Bondar, Izv. Akad. Nauk SSSR, Otd. Khim. Nauk 8 (1961) 1372.
[30] L.J. Gaukler, H. Hohnke, T.Y. Tien, J. Am. Ceram. Soc. 63 (1980) 35–37.
[31] G.S. Painter, P.F. Becher, W.A. Shelton, R.L. Satet, M.J. Hoffman, Phys. Rev. B 70 (2004) 144108.
[32] G.B. Winkelman, C. Dwyer, T.S. Hudson, D. Nguyen-Manh, M. Döblinger, R.L. Satet, M.J. Hoffman, D.J. Cockayne, App. Phys. Lett., 87 (2005) 061911.
[33] N. Shibata, S.J. Pennycook, T.R. Gosnell, G.S. Painter, W.A. Shelton, P.F. Becher, Nature 428 (2004) 730–733.
[34] A. Ziegler, J.C. Idrobo, M.K. Cinibulk, C. Kisielowski, N.D. Browning, R.O. Ritchie, Science 306 (2004) 1768–1770.

[35] P.F. Becher, G.S. Painter, S.B. Waters, H.-T. Lin, N. Shibata, Effect of rare earth (RE) adsorption on the phase transformation and microstructure evolution in silicon nitride with RE_2O_3 + MgO additives and the resultant fracture behavior, J. Am. Ceram. Soc., submitted.
[36] M. Quinlan, D. Heard, L. Garrido, L. Genova, K.P. Plucknett, Ceram. Eng. Sci. Proc. 28 (2007) 41–48.
[37] M. Quinlan, L. Garrido, L. Genova, K.P. Plucknett, Ceram. Eng. Sci. Proc. 28 (2007) 49–56.
[38] N. Saito, D. Nakata, A. Umemoto, K. Nakashima, in: H.-D. Kim, H.-T. Lin, M.J. Hoffmann (Eds.), Advanced Si-Based Ceramics and Composites, Key Engineering Materials, vol. 287, Trans Tech Publications, Zurich, Switzerland, 2005, pp. 265–270.
[39] R.L. Satet, M.J. Hoffmann, J. Eur. Ceram. Soc. 24 (2004) 3437–3445.
[40] R.L. Satet, M.J. Hoffmann, R.M. Cannon, Mater. Sci. Eng. A422 (2006) 66–76.
[41] P.F. Becher, G.S. Painter, N. Shibata, R.L. Satet, M.J. Hoffmann, S.J. Pennycook, Mater. Sci. Eng. A422 (2006) 85–91.
[42] M. Quinlan, D. Gould, L. Garrido, L. Genova K.P. Plucknett, The effects of milling time on the sintering response of porous β-Si_3N_4 ceramics, Ceram. Int., in preparation.